

Supporting Information for

Ba₆In₂Ge₂Te₁₅: a THz birefringent material with an intriguing quasi-[Te₅]⁴⁻ chain possessing giant optical anisotropy and ultrawide transmission range

Mengran Sun,^{a,b,c} Xingyu Zhang,^{b,c,d} Wenhao Xing,^e Ece Uykur,^f Wenlong Yin,^e

Zheshuai Lin,^d and Jiyong Yao^{a,*}

^a Center for Crystal Research and Development, Key Lab of Functional Crystals and Laser Technology, Technical Institute of Physics and Chemistry, Chinese Academy of Sciences, Beijing 100190, P. R. China.

^b Center of Materials Science and Optoelectronics Engineering, University of Chinese Academy of Sciences, Beijing 100049, P. R. China.

^c University of Chinese Academy of Sciences, Beijing 100049, P. R. China.

^d Functional Crystals Lab, Technical Institute of Physics and Chemistry, Chinese Academy of Sciences, Beijing 100190, China.

^e Institute of Chemical Materials, China Academy of Engineering Physics, Mianyang 621900, P. R. China.

^f Physikalisches Institut, Universität Stuttgart, 70569 Stuttgart, Germany.

*Corresponding author:

Jiyong Yao; jyao@mail.ipc.ac.cn.

1. Synthesis of $\text{Ba}_6\text{In}_2\text{Ge}_2\text{Te}_{15}$ single crystal
2. Structure determination
3. Synthesis of $\text{Ba}_6\text{In}_2\text{Ge}_2\text{Te}_{15}$ polycrystalline powder
4. Properties characterization
5. Computational methods
6. Figure S1. The powder XRD pattern of $\text{Ba}_6\text{In}_2\text{Ge}_2\text{Te}_{15}$
7. Figure S2. The element analysis of $\text{Ba}_6\text{In}_2\text{Ge}_2\text{Te}_{15}$
8. Figure S3. Coordination modes of Ba atoms in $\text{Ba}_6\text{In}_2\text{Ge}_2\text{Te}_{15}$
9. Figure S4. IR and raman spectra of $\text{Ba}_6\text{In}_2\text{Ge}_2\text{Te}_{15}$ powder
10. Figure S5. UV-vis-NIR diffuse-reflectance spectrum of $\text{Ba}_6\text{In}_2\text{Ge}_2\text{Te}_{15}$ powder
11. Figure S6. Differential scanning calorimetry curve of $\text{Ba}_6\text{In}_2\text{Ge}_2\text{Te}_{15}$ powder
12. Table S1. Crystallographic data and structure refinement for $\text{Ba}_6\text{In}_2\text{Ge}_2\text{Te}_{15}$
13. Table S2. Atomic coordinates, equivalent isotropic displacement parameters, and Wyckoff site for $\text{Ba}_6\text{Ge}_2\text{In}_2\text{Te}_{15}$
14. Table S3. Selected bond Lengths and angles for $\text{Ba}_6\text{Ge}_2\text{In}_2\text{Te}_{15}$

Experimental details

Reagent. All starting materials, Ba (99.99%), In (99.99%), Ge (99.99%), and Te (99.999%) were directly purchased from Aladdin Co., Ltd. without further purification. The synthesis of binary materials BaTe, In₂Te₃, and GeTe are to heat the stoichiometric mixture of the elements in vacuum flame-sealed silica tubes. All manipulations are carried out in an Ar-filled glove box.

1. Single Crystal Synthesis

The Ba₆In₂Ge₂Te₁₅ single crystals were grown via spontaneously crystallization. BaTe (0.944mmol, 0.25g), In₂Te₃ (0.135mmol, 0.083g), GeTe (0.674mmol, 0.135g), and Te (0.270mmol, 0.034g) were thoroughly ground and loaded into a quartz tube. The tube containing the raw materials was sealed under a 10⁻³ pa vacuum and placed in a tube furnace. Then, set the heating program as follows: the tube was heated from room temperature to 1173 K in 20 h, kept for 50 h, then slowly cooled to 773 K at a rate of 3 K/h, and finally cooled to room temperature within 5h. The metallic plate-like crystals of Ba₆In₂Ge₂Te₁₅ can be obtained with a yield of 60% (base on Ge). These crystals are not sensitive to oxygen and water in the air.

2. Structure Determination

A Ba₆In₂Ge₂Te₁₅ crystal without cracks was selected for single-crystal X-ray diffraction on a XtaLAB Synergy four-circle diffractometer equipped with a graphite-monochromated Mo-K_α (λ = 0.71073 Å) radiation at 297(2) K. CrysAlispro software was used for data reduction, and Multi-scan method was used for absorption

correction. Structure solution and refinement of $\text{Ba}_6\text{In}_2\text{Ge}_2\text{Te}_{15}$ were carried out with the direct method and full-matrix least squares on F^2 with SHELXL-2014.¹ The crystallographic data and structure refinement details of $\text{Ba}_6\text{In}_2\text{Ge}_2\text{Te}_{15}$ are exhibited in Table S1. The atomic coordinates, equivalent isotropic displacement parameters, and Wyckoff sites are listed in Table S2. The selected bond lengths and angles are summarized in Table S3.

3. Polycrystalline Synthesis

The polycrystalline powder of $\text{Ba}_6\text{In}_2\text{Ge}_2\text{Te}_{15}$ adopts the traditional high-temperature solid-state synthesis method by heating the stoichiometric mixture of the elements. The mixture of 0.25 g BaTe, 0.096 g In_2Ge_3 , 0.063 g GeTe, and 0.08 g Te was evenly ground and placed into a quartz tube, which was sealed under high vacuum of 10^{-3} Pa. This sample were gradually heated to 823 K in 10 h, maintained for 50 h, and finally cooled to room temperature (RT).

4. Properties Characterization

Powder X-ray Diffraction

A Bruker D8 Focus diffractometer equipped with Cu-K_α ($\lambda = 1.5418 \text{ \AA}$) radiation was used to perform the powder X-ray diffraction of $\text{Ba}_6\text{In}_2\text{Ge}_2\text{Te}_{15}$. The diffraction pattern from 10° to 70° was collected with the parameters of a scanning step width of 0.02° and a counting time of 0.1 s/step.

Element Analysis

The FEI Quanta 650FEG scanning electron microscope (SEM) equipped with energy-dispersive X-ray (EDX) was used to perform the elemental analysis on the single crystal of $\text{Ba}_6\text{In}_2\text{Ge}_2\text{Te}_{15}$.

Optical Characterizations

A Carry 5000 UV-vis-NIR spectrophotometer with a diffuse reflectance accessory was applied to obtain the diffuse-reflectance spectrum of $\text{Ba}_6\text{In}_2\text{Ge}_2\text{Te}_{15}$ and BaSO_4 (as a reference) in the range of 2500 – 200 nm. A Lab RAM Aramis spectrometer equipped with a 532 nm laser was used to collect the Raman spectrum of $\text{Ba}_6\text{In}_2\text{Ge}_2\text{Te}_{15}$ in the range of 100 to 1000 cm^{-1} at RT. A Excalibur 3100 Fourier Transform Infrared Spectrometer was used to collect the IR spectrum in the range of 400-4000 cm^{-1} . The samples for IR measurement were prepared by fully grinding $\text{Ba}_6\text{In}_2\text{Ge}_2\text{Te}_{15}$ crystals with KBr powder (1:100 mass ratio). Moreover, single crystal of $\text{Ba}_6\text{In}_2\text{Ge}_2\text{Te}_{15}$ with a size of 1 mm \times 0.42 mm \times 0.1 mm was used to perform transmission measurements. Room-temperature transmission measurements are performed in the frequency range of 0.8–71 μm . The spectra are collected with the Vertex80 Bruker Fourier transform infrared spectrometer that is coupled to a Hyperion infrared microscope allowing us to measure micrometer-size samples. During the measurements, the infrared microscope and sample environment were purged with nitrogen, while the infrared spectrometer itself was under vacuum. A global light source is used in the measurements. An MCT nitrogen-cooled detector has been utilized for the measurements in the 0.8–16 μm range, while for the 15–71 μm frequency range, a helium-cooled bolometer is used. Overlapping regions allow

us to merge the spectra reliably.

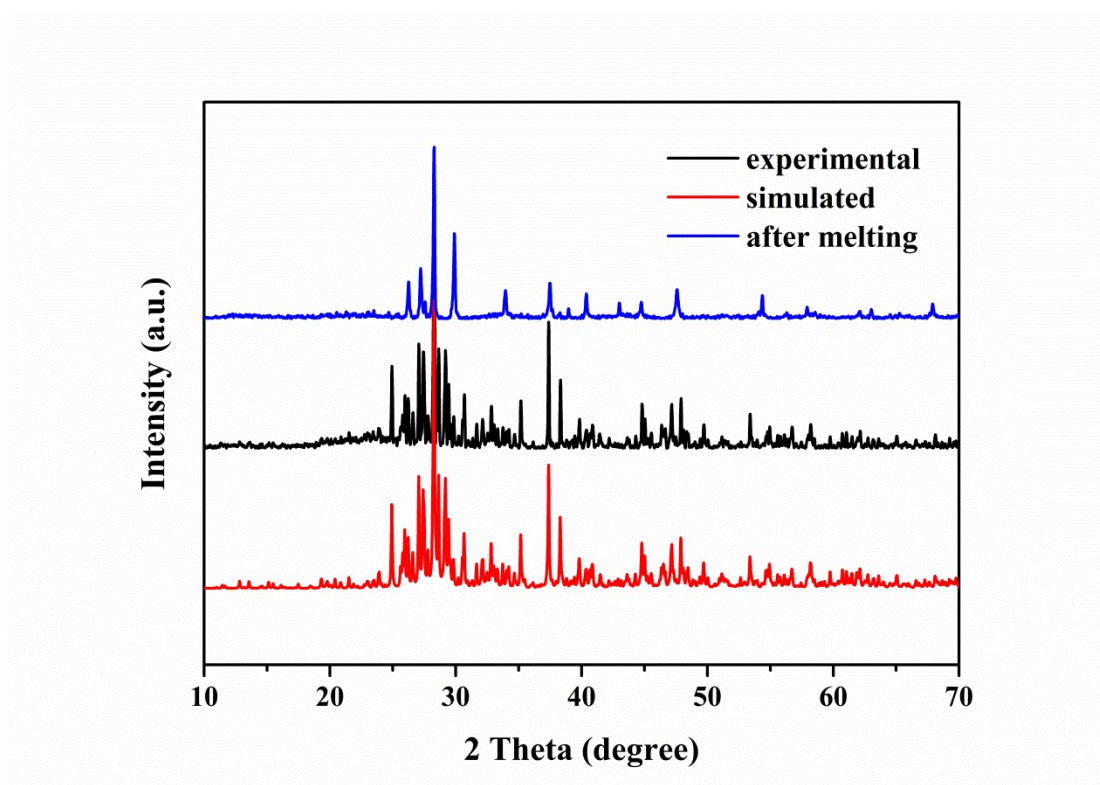
Thermal Properties

A Labsys TG-DTA16 (SETARAM) thermal analyzer was used to evaluate the thermal stability of $\text{Ba}_6\text{In}_2\text{Ge}_2\text{Te}_{15}$. Appropriate amount of $\text{Ba}_6\text{In}_2\text{Ge}_2\text{Te}_{15}$ polycrystalline powder was placed into a quartz tube with the size of 5 mm (o.d.) \times 3 mm (i.d.) and eventually sealed the tube at 10^{-6} Pa. During the measurement process, the nitrogen flow was circulated at a flow rate of about 15 mL/ min, and the temperature of the tube was heated from RT to 1273 K at a rate of 15 K / min, and then gradually lowered to RT at the same rate.

5. Theoretical Calculations

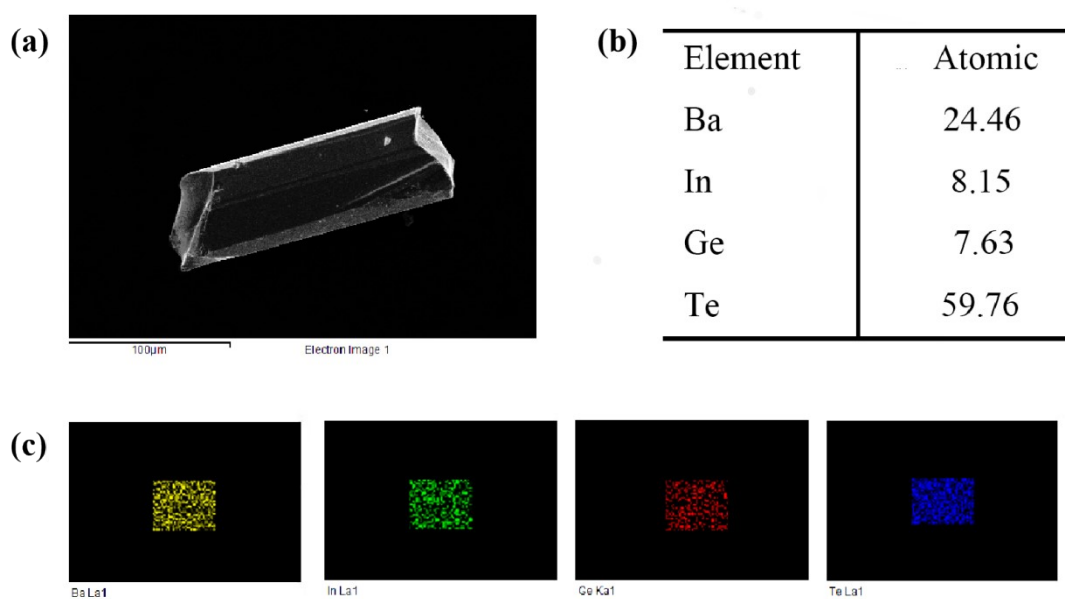
The First-principles Calculations were performed by the method of plane-wave pseudo potential in the CASTEP package according to density functional theory (DFT).²⁻³ The Perdew-Burke-Ernzerhof (PBE) function was used to describe the exchange-related energy in the generalized gradient approximation (GGA) with a 600 eV kinetic energy cutoff.⁴⁻⁵ The norm-conserving pseudopotential was chosen to simulate the interaction between the atom cores and the valence electrons with a small plane-wave basis.⁶ And the total valence electrons are distributed as Ba $5s^25p^66s^2$, In $5s^25p^1$ Ge $4s^24p^2$, Te $5s^25p^4$ electrons. The dense Monkhorst-Pack κ -point meshes was selected to $3\times 2\times 1$ for $\text{Ba}_6\text{In}_2\text{Ge}_2\text{Te}_{15}$ in the numerically integration of the Brillouin zone.⁷ The optical properties were calculated by the shift of conduction band (CB) with the scissor operation to match the experimental value.⁸ The refractive index was calculated based on the Kramers-Kronics transform.

6. Figure S1



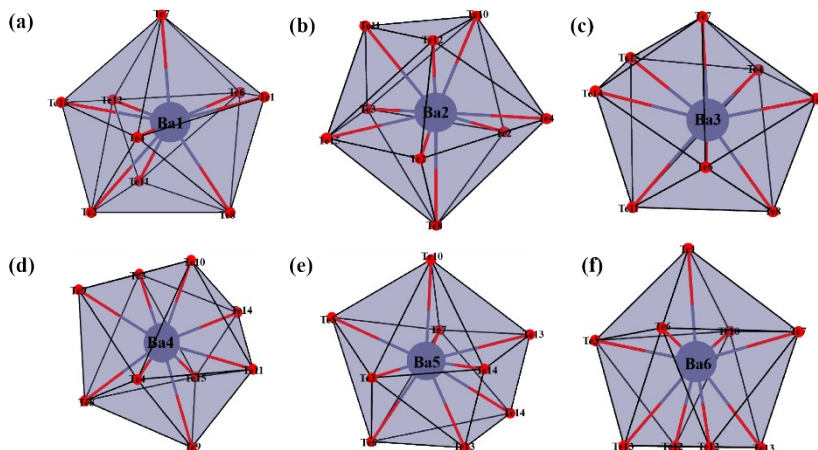
Experimental (black), simulated (red) and after melting (blue) PXR D patterns of $\text{Ba}_6\text{In}_2\text{Ge}_2\text{Te}_{15}$.

7. Figure S2



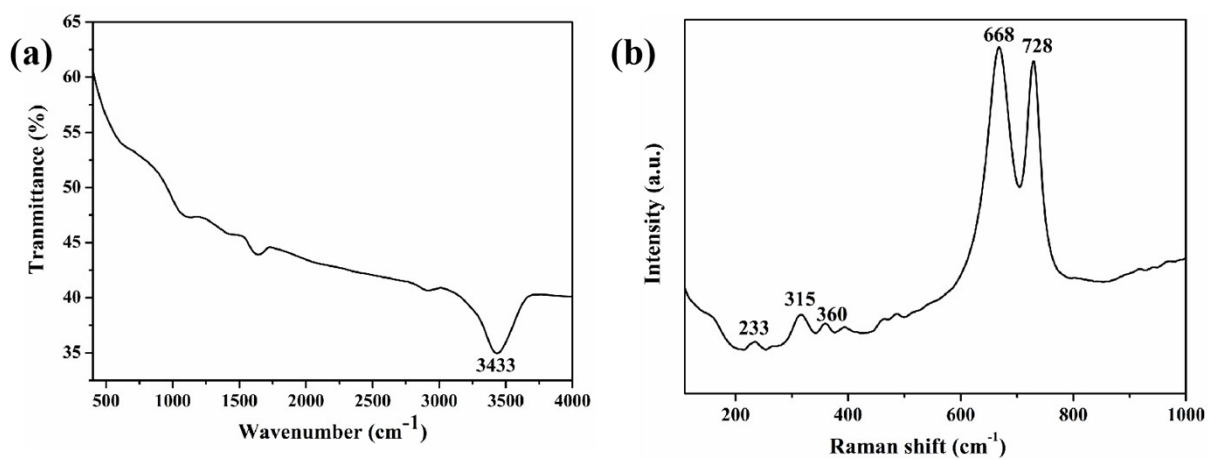
(a) Scanning electron microscopy (SEM) image of $\text{Ba}_6\text{In}_2\text{Ge}_2\text{Te}_{15}$; (b) Elemental analysis of $\text{Ba}_6\text{In}_2\text{Ge}_2\text{Te}_{15}$ by EDX spectroscopy. (c) Elemental distribution of the as-grown crystal (from left to right: Ba, In, Ge, Te).

8. Figure S3



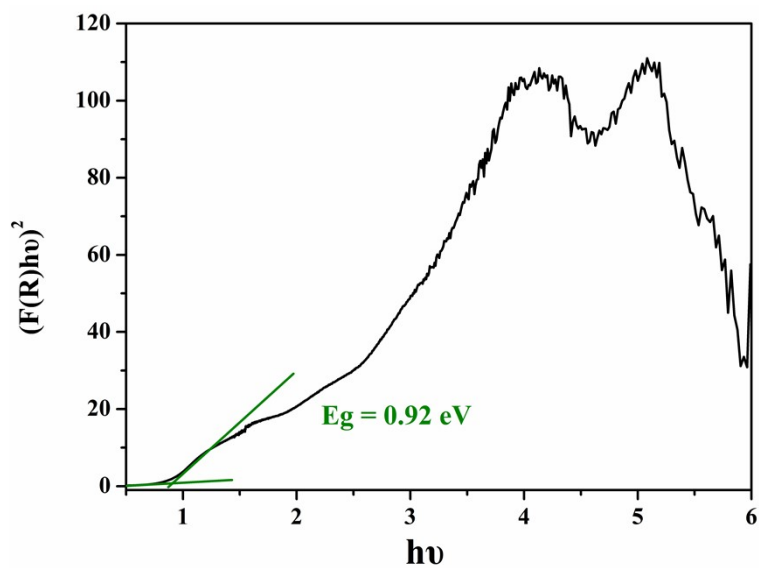
Coordination modes of Ba1 (a), Ba2 (b), Ba3 (c), Ba4 (d), Ba5 (e), and Ba6 (f).

9. Figure S4



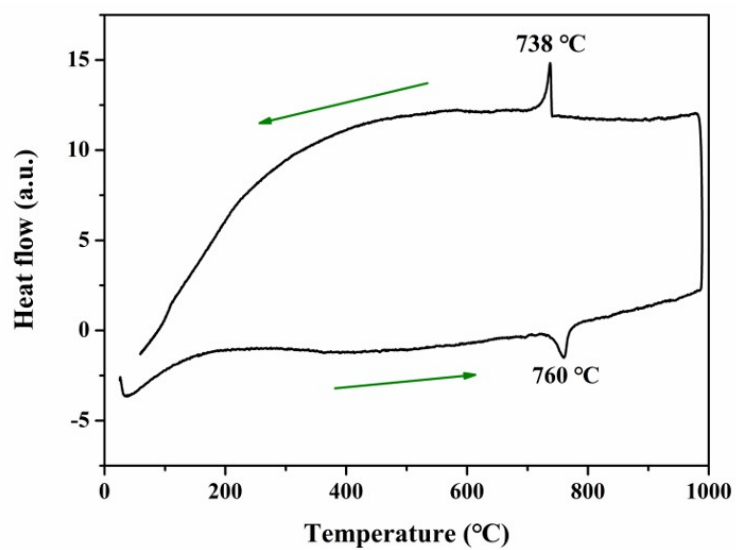
(a) IR spectrum of $\text{Ba}_6\text{In}_2\text{Ge}_2\text{Te}_{15}$ powder. (b) Raman spectrum of $\text{Ba}_6\text{In}_2\text{Ge}_2\text{Te}_{15}$ powder.

10. Figure S5



UV-vis-NIR diffuse-reflectance spectrum (Inset: the polycrystalline powder of $\text{Ba}_6\text{In}_2\text{Ge}_2\text{Te}_{15}$).

11. Figure S6



Differential scanning calorimetry (DSC) curve of $\text{Ba}_6\text{In}_2\text{Ge}_2\text{Te}_{15}$.

12. Table S1 Crystallographic data and structure refinement for Ba₆In₂Ge₂Te₁₅.

Empirical formula	Ba ₆ Ge ₂ In ₂ Te ₁₅
Formula Weight	3112.86
Crystal System	monoclinic
Space Group	<i>P2₁/c</i>
<i>T</i> /K	296(2)
<i>a</i> (Å)	9.6201(6)
<i>b</i> (Å)	13.4225(7)
<i>c</i> (Å)	27.5845(16)
α (°)	90
β (°)	92.469(2)
γ (°)	90
<i>V</i> (Å ³)	3558.6(4)
<i>Z</i>	4
ρ_{calc} (g/cm ³)	5.810
<i>M</i> (mm ⁻¹)	21.505
Radiation	Mo K α (λ =0.71073)
2θ range for data	2.956 to 61.058
Index ranges	-13 \leq h \leq 13, -18 \leq k \leq 19, -39 \leq l \leq 39
Reflections collected	10847
Independent reflections	[R _{int} = 0.0852, R _{sigma} =0.0734]
GoF on F ²	1.080
Final R indexes [<i>I</i> \geq 2 σ (<i>I</i>)]	R ₁ = 0.0512, wR ₂ = 0.0804
Final R indexes [all data]	R ₁ = 0.0856, wR ₂ = 0.0896

13. Table S2 Atomic Coordinates ($\times 10^4$), equivalent isotropic displacement parameters $(\text{\AA}^2 \times 10^3)$, and Wyckoff site for $\text{Ba}_6\text{Ge}_2\text{In}_2\text{Te}_{15}$.

Atom	Wyckoff site	x	y	z	U_{eq}
Ba1	4e	5016.2(7)	3158.9(5)	3709.2(3)	13.60(15)
Ba2	4e	5075.0(7)	4583.5(5)	2004.6(3)	12.24(15)
Ba3	4e	10067.7(7)	3119.2(5)	3738.8(3)	12.81(15)
Ba4	4e	9917.1(7)	9482.6(5)	3025.8(3)	11.80(14)
Ba5	4e	9947.0(7)	8086.5(5)	4640.0(3)	11.70(14)
Ba6	4e	4913.9(7)	8111.2(5)	4662.8(3)	11.93(14)
In1	4e	7490.4(9)	5278.0(6)	4625.3(3)	14.25(18)
In2	4e	2340.7(9)	6454.2(6)	3114.3(3)	15.41(19)
Ge1	4e	6319.2(13)	6737.7(9)	3407.1(5)	11.7(3)
Ge2	4e	8395.3(13)	5824.8(9)	3225.5(5)	11.9(3)
Te1	4e	5029.2(8)	5735.1(5)	4053.6(3)	13.15(16)
Te2	4e	4804.2(8)	6981.6(5)	2608.6(3)	12.53(16)
Te3	4e	7273.3(8)	8378.5(5)	3747.5(3)	10.99(15)
Te4	4e	7661.9(8)	4102.0(5)	2903.6(3)	12.04(16)
Te5	4e	9818.3(8)	5699.7(5)	4045.1(3)	12.98(16)
Te6	4e	7451.0(8)	6720.8(6)	5324.3(3)	13.96(16)
Te7	4e	7539.0(8)	3245.8(5)	4674.5(3)	13.48(16)
Te8	4e	2473.2(8)	4411.5(5)	2981.1(3)	13.19(16)
Te9	4e	-288.2(8)	6867.4(5)	2600.5(3)	12.73(16)
Te10	4e	2399.9(8)	8112.3(5)	3708.7(3)	11.92(16)
Te11	4e	7453.8(8)	8713.5(5)	6575.5(3)	14.10(17)
Te12	4e	5661.4(8)	9333.2(5)	5812.0(3)	13.05(16)
Te13	4e	7518.5(8)	9992.3(5)	5024.6(3)	15.25(17)
Te14	4e	9379.9(8)	10648.1(5)	4195.3(3)	12.73(16)
Te15	4e	7580.8(8)	11288.3(5)	3433.4(3)	13.25(16)

14. Table S3 Selected Bond Lengths (Å) and Angles (°) for Ba₆Ge₂In₂Te₁₅.

Lengths(Å)			
Ge1—Ge2	2.4141(17)	In1—Te7	2.7314(11)
Ge1—Te1	2.5927(15)	In2—Te2	2.8893(12)
Ge1—Te2	2.6088(15)	In2—Te8	2.7699(11)
Ge1—Te3	2.5495(14)	In2—Te9	2.8989(12)
Ge2—Te4	2.5651(14)	In2—Te10	2.7635(11)
Ge2—Te5	2.5975(15)	Te11—Te12	2.7905(11)
Ge2—Te9 ¹	2.5927(15)	Te12—Te13	3.0045(12)
In1—Te1	2.8545(12)	Te13—Te14	3.0931(12)
In1—Te5	2.8646(12)	Te14—Te15	2.7996(11)
In1—Te6	2.7342(11)		

Angles(°)			
Te1—In1—Te5	107.38(4)	Te3—Ge1—Te2	112.44(5)
Te7—In1—Te1	104.72(4)	Te1—Ge1—Te2	112.29(5)
Te7—In1—Te5	102.30(4)	Ge1—Ge2—Te4	108.16(6)
Te7—In1—Te6	132.30(4)	Ge1—Ge2—Te5	105.18(6)
Te6—In1—Te1	101.60(3)	Ge1—Ge2—Te9	107.23(6)
Te6—In1—Te5	106.80(4)	Ge2—Ge1—Te3	103.12(6)
Te10—In2—Te9	97.54(3)	Ge2—Ge1—Te1	107.70(6)
Te10—In2—Te8	151.16(4)	Ge2—Ge1—Te2	109.00(6)
Te10—In2—Te8	151.16(4)	Te9—Ge2—Te5	111.07(5)
Te10—In2—Te2	95.32(3)	Te4—Ge2—Te9	113.04(5)
Te8—In2—Te9	99.71(3)	Te4—Ge2—Te5	111.70(5)
Te8—In2—Te2	97.77(3)	Te11—Te12—Te13	105.43(3)
Te2—In2—Te9	115.69(4)	Te12—Te13—Te14	178.60(4)
Te3—Ge1—Te1	111.74(5)	Te13—Te14—Te15	106.48(3)

¹1+x,+y,+z; ²2-x,1-y,1-z; ³2-x,2-y,1-z; ⁴-1+x,+y,+z; ⁵1-x,1-y,1-z; ⁶+x,-1+y,+z;

⁷1-x,-1/2+y,1/2-z; ⁸1-x,2-y,1-z; ⁹2-x,-1/2+y,1/2-z; ¹⁰+x,3/2-y,-1/2+z; ¹¹2-x,1/2+y,1/2-z;

¹²1-x,1/2+y,1/2-z; ¹³+x,1+y,+z; ¹⁴+x,3/2-y,1/2+z.

Reference

1. Sheldrick, G., Crystal structure refinement with SHELXL. *Acta Crystallogr. C* **2015**, *71* (1), 3-8.
2. Clark, S. J.; Segall, M. D.; Pickard, C. J.; Hasnip, P. J.; Probert, M. I. J.; Refson, K.; Payne, M. C., First principles methods using CASTEP. *Z. Krist.- Cryst. Mater.* **2005**, *220* (5-6), 567-570.
3. Segall, M. D.; Lindan, P. J. D.; Probert, M. J.; Pickard, C. J.; Hasnip, P. J.; Clark, S. J.; Payne, M. C., First-principles simulation: ideas, illustrations and the CASTEP code. *J. Phys. Condens. Matter* **2002**, *14* (11), 2717-2744.
4. Ceperley, D. M.; Alder, B. J., Ground State of the Electron Gas by a Stochastic Method. *Phys. Rev. Lett.* **1980**, *45* (7), 566-569.
5. Perdew, J. P.; Zunger, A., Self-interaction correction to density-functional approximations for many-electron systems. *Phys. Rev. B* **1981**, *23* (10), 5048-5079.
6. Rappe, A. M.; Rabe, K. M.; Kaxiras, E.; Joannopoulos, J. D., Optimized pseudopotentials. *Phys. Rev. B* **1990**, *41* (2), 1227-1230.
7. Monkhorst, H. J.; Pack, J. D., Special points for Brillouin-zone integrations. *Phys. Rev. B* **1976**, *13* (12), 5188-5192.
8. Godby, R. W.; Schlüter, M.; Sham, L. J., Self-energy operators and exchange-correlation potentials in semiconductors. *Phys. Rev. B* **1988**, *37* (17), 10159-10175.